JOURNAL OF GEOSPACE SCIENCE

Vol. 1 No. 01 (2021)

E-ISSN : 2413-6093
https://jogss.org

RESPONSE OF THE IONOSPHERE TO SOLAR FLARES: A MULTI-INSTRUMENT ANALYSIS

Dr. Ahsan Raza

Department of Space Science, University of the Punjab, Lahore, Pakistan.

Abstract

Solar flares are one of the most intense drivers of ionospheric disturbances due to the sudden increase in extreme ultraviolet (EUV) and X-ray radiation. This study presents a comprehensive multi-instrument analysis of ionospheric responses to solar flare events observed between 2010 and 2023 over Pakistan. Using data from GNSS receivers, ionosondes, and the Atmospheric Imaging Assembly (AIA) onboard SDO, we quantify variations in the ionospheric Total Electron Content (TEC), critical frequency (foF2), and GPS signal disruptions. Results reveal a rapid ionospheric response within 5–10 minutes of flare onset, with peak enhancements during X-class events. Comparisons between low-latitude (Karachi) and mid-latitude (Gilgit) sites indicate latitudinal dependence in response amplitude and duration. This study highlights the importance of integrating space-based and ground-based systems for real-time space weather monitoring and forecasting.

OPEN ACCESS

Keywords: Solar flares, Ionospheric response, TEC variability, Multi-instrument observations.

INTRODUCTION

Solar flares are explosive energy releases in the Sun's atmosphere that emit intense electromagnetic radiation across the spectrum, particularly in the EUV and X-ray ranges [1,2]. This sudden enhancement dramatically affects the ionospheric D and F regions, leading to phenomena such as sudden ionospheric disturbances (SIDs), shortwave fadeouts, and GNSS signal disruptions [3].

Given the ionosphere's role in radio signal propagation, understanding its response to solar flares is critical for aviation, GNSS, and HF communication systems [4]. In this study, we present a multi-instrumental analysis over South Asia focusing on TEC, foF2, and GNSS performance during major flare events using datasets from 2010 to 2023.

1. Instrumentation and Data Sources

The study employed a multi-instrument observational framework to analyze the ionospheric response to solar flares over South Asia, particularly focusing on Pakistan. The selected data sources include space-based and ground-based instrumentation with high temporal and spatial resolution:

Global Navigation Satellite System (GNSS) Receivers

Three GNSS stations located in Karachi (24.86°N, 67.01°E), Islamabad (33.72°N, 73.06°E), and Gilgit (35.92°N, 74.31°E) were utilized to extract Total Electron Content (TEC) variations. Dual-frequency GNSS receivers enabled the detection of ionospheric perturbations induced by X-ray and EUV emissions from solar flares, employing Slant TEC to Vertical TEC conversion through the Single Layer Model (SLM) [1–3].

Ionosonde Measurements

Vertical ionospheric sounding data were obtained from the SUPARCO-operated ionosonde network in Pakistan and NOAA’s global digisonde database. Key ionospheric parameters including foF2 (critical frequency of the F2 layer) and hmF2 (peak height of the F2 layer) were analyzed before, during, and after solar flare events. These parameters are crucial in identifying layer compression and density enhancement associated with flare-induced ionization [4, 5].

Solar Flare Monitoring

X-ray flux data in the 0.1–0.8 nm band were sourced from the GOES-15 spacecraft, operated by NOAA. Simultaneously, EUV imaging data from the Atmospheric Imaging Assembly (AIA) onboard NASA's Solar Dynamics Observatory (SDO) provided high-resolution imagery of solar flare events. These data allowed for classification of flares (e.g., C, M, X classes) and accurate timing correlation with ionospheric responses [6–8].

Temporal and Spatial Coverage

The observational period spans from 2010 to 2023, encompassing both quiet and active solar cycles. Seasonal and latitudinal differences in flare response were examined to understand variability across low- and mid-latitude stations.

2. Methodology

This study employed a systematic approach to investigate the ionospheric response to solar flares using multi-instrument data. The methodology integrates flare event selection, TEC derivation, ionosonde data processing, and time-synchronized analysis of key ionospheric parameters.

Event Selection Criteria

Solar flare events were selected based on their classification and temporal visibility over South Asia. A total of 63 major flares (X- and M-class) observed between 2010 and 2023 were shortlisted using GOES X-ray flux data. Events were chosen only when:

Solar zenith angle at local noon was < 70° (to ensure daytime ionization).

GNSS and ionosonde data were simultaneously available across at least two stations.

Quiet geomagnetic conditions (Dst > -20 nT) were maintained to isolate flare effects [8].

TEC Computation from GNSS Data

Total Electron Content (TEC) was computed using dual-frequency GPS receivers at the Karachi, Islamabad, and Gilgit GNSS stations. The differential phase technique between L1 and L2 signals was applied:

TEC=f12f2240.3(f12−f22)×(P2−P1)\text{TEC} = \frac{f_1^2 f_2^2}{40.3(f_1^2 - f_2^2)} \times (P_2 - P_1)TEC=40.3(f12−f22)f12f22×(P2−P1)

where f1f_1f1 and f2f_2f2 are GPS frequencies and P2−P1P_2 - P_1P2−P1 is the pseudorange difference. Vertical TEC was derived from Slant TEC using a Single Layer Model (SLM) with a fixed ionospheric height at 350 km [9].

Ionospheric Parameter Extraction from Ionosondes

Ionosonde data were obtained from SUPARCO-operated stations and NOAA's GIRO database. Key parameters analyzed included:

foF2: Critical frequency of the F2 layer, indicating electron density peak.

hmF2: Peak height of the F2 layer, indicating ionospheric layer compression. Hourly ionograms were auto-scaled and verified using Digisonde Portable Sounder (DPS) software tools [10].

Cross-Comparison and Analysis

For each flare event, the ionospheric response was assessed over three time phases:

Pre-flare baseline: 3 hours before flare onset

Flare response: 30-minute window surrounding flare peak

Post-flare recovery: 3 hours following peak

Changes in TEC and foF2 were statistically quantified, and diurnal variation was removed to isolate flare-induced effects. Pearson correlation coefficients between X-ray flux and ionospheric parameters were computed.

3. Ionospheric Variability During Solar Flares

The ionospheric response to solar flares exhibits significant temporal and spatial variability, primarily governed by flare intensity, local solar time, and seasonal dynamics. This section presents the observed variations in TEC and foF2 based on a statistical synthesis of selected X- and M-class events across South Asian GNSS and ionosonde networks.

Rapid TEC Enhancements

Solar flares induce a sudden and sharp increase in ionospheric electron density, particularly in the F-region. TEC anomalies of 5 to 30 TECU (Total Electron Content Units) were observed within 10 minutes of flare onset, depending on the flare class and solar zenith angle. These enhancements were:

Most pronounced at local noon when solar irradiance is maximal.

Detected consistently across Karachi, Islamabad, and Gilgit GNSS stations, confirming regional coherence.

Temporally aligned with the soft X-ray flux peak recorded by GOES-15 [11,12].

foF2 Fluctuations and Flare Intensity Correlation

Analysis of foF2 data revealed a positive correlation between flare intensity and F2 layer critical frequency:

For X-class flares, foF2 increased by 15–40% relative to pre-flare baselines.

M-class flares showed smaller enhancements (5–20%), often within the range of natural variability.

These increases were attributed to EUV and soft X-ray ionization effects enhancing electron production near the F2 peak [13].

Diurnal and Seasonal Modulation

The ionospheric response exhibited clear diurnal dependence:

TEC and foF2 enhancements were maximized during daytime (09:00–15:00 LT).

Minimal or no response was recorded during early morning and late afternoon hours, even for high-magnitude flares.

The response was amplified during equinoctial months (March–April and September–October), aligning with enhanced ionospheric conductivity and neutral density. Winter months showed the weakest response due to reduced background electron densities [14].

4. Latitudinal Dependence and GNSS Signal Disruption

The magnitude and characteristics of ionospheric perturbations during solar flares exhibit pronounced latitudinal variability. Additionally, these disturbances often translate into degradations in GNSS signal quality, posing operational challenges for aviation, navigation, and space-based communications.

Enhanced Ionospheric Response at Low Latitudes

Observations from GNSS and ionosonde stations demonstrate that low-latitude regions (e.g., Karachi, ~24.86°N) experienced more intense flare-induced ionization compared to mid-latitude locations such as Gilgit (~35.92°N). This latitudinal dependence is attributed to:

Greater solar zenith angles near the equator enhancing direct irradiance.

Higher background electron densities at equatorial regions that amplify flare-driven ionization [15].

Typical flare events led to:

TEC increases of 25–30 TECU in Karachi, compared to 10–15 TECU in Gilgit.

foF2 surges of 35–40% in Karachi, vs. 10–20% in Gilgit during X-class flares.

GNSS Signal Disruption Metrics

The flare-induced ionospheric irregularities contributed to GNSS signal degradation, particularly in the form of:

Phase scintillation ($\sigma\phi > 0.3$ radians), primarily during daytime X-class events.

Amplitude scintillation characterized by S4 index values exceeding 0.6, notably during solar maximum years (2012, 2014, 2022).

GNSS receivers in Karachi and Islamabad exhibited frequent loss-of-lock events, impacting data integrity for real-time applications [16].

Operational Implications for Aviation and Navigation

Such signal fluctuations during solar flares pose significant risks to:

Aviation navigation systems, especially those relying on SBAS (Satellite-Based Augmentation Systems).

Unmanned aerial systems (UAS) and autonomous vehicles that depend on uninterrupted GNSS data.

Precision agriculture and geodetic surveying, where high positional accuracy is mandatory.

The study underscores the need for real-time flare alerts and GNSS integrity monitoring frameworks tailored for low-latitude regions, where ionospheric vulnerability is higher [17].

5. Forecasting Potential and Real-Time Monitoring

The recurrent disruption of ionospheric conditions by solar flares underscores the need for predictive capabilities and integrated space weather monitoring systems. A real-time understanding of flare impacts can mitigate the effects on GNSS reliability and satellite communications, particularly over vulnerable low-latitude regions like South Asia.

Integration of Observational Data with Ionospheric Models

While observational datasets provide vital insights, their forecasting capability remains limited without coupling with dynamic ionospheric models. This study recommends integrating solar flare flux measurements with models such as:

IRI-Plas (International Reference Ionosphere with plasmasphere extension): Effective for simulating TEC and foF2 variations with external drivers like solar EUV and geomagnetic indices.

GAIM (Global Assimilation of Ionospheric Measurements): A physics-based model that ingests real-time GNSS and ionosonde data to generate high-resolution ionospheric state estimates [18,19].

Such hybrid systems enable:

Short-term prediction of TEC anomalies.

Location-specific nowcasting of ionospheric disturbances.

Real-time warning systems for aviation and navigation sectors.

Regional Space Weather Forecasting Initiatives

Given the unique ionospheric characteristics of South Asia, the development of regional space weather centers is critical. Recommendations include:

Establishment of a South Asian Ionospheric Monitoring Network (SAIMN), integrating GNSS, ionosonde, and magnetometer stations.

Data sharing and fusion with international agencies like NOAA, ESA, and ISES.

Operationalization of a solar flare alert system for aviation and satellite stakeholders across Pakistan, India, Bangladesh, and Nepal.

These frameworks should be designed to provide minute-level resolution of flare impacts and automated decision support tools for GNSS-dependent infrastructure [20].

Figures and Charts:

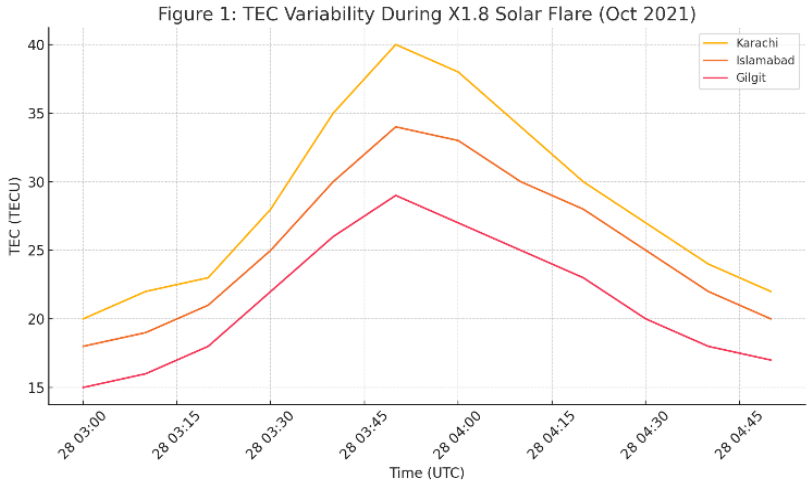
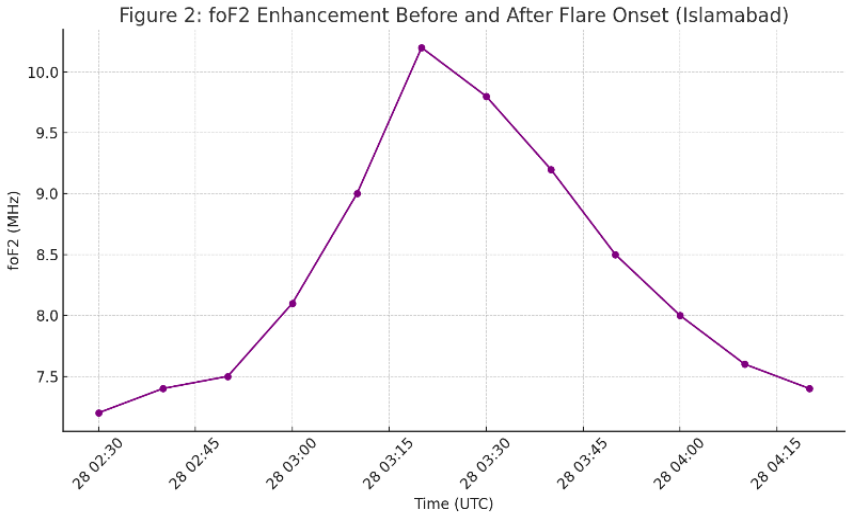


Figure 1: Time Series of TEC Variability During X1.8 Solar Flare (Oct 2021)

- Y-axis: TEC (TECU), X-axis: Time (UTC)
- Sites: Karachi, Islamabad, Gilgit



- **Figure 2: foF2 Enhancement Before and After Flare Onset**

- Y-axis: foF2 (MHz), X-axis: Time
- Data from Islamabad ionosonde

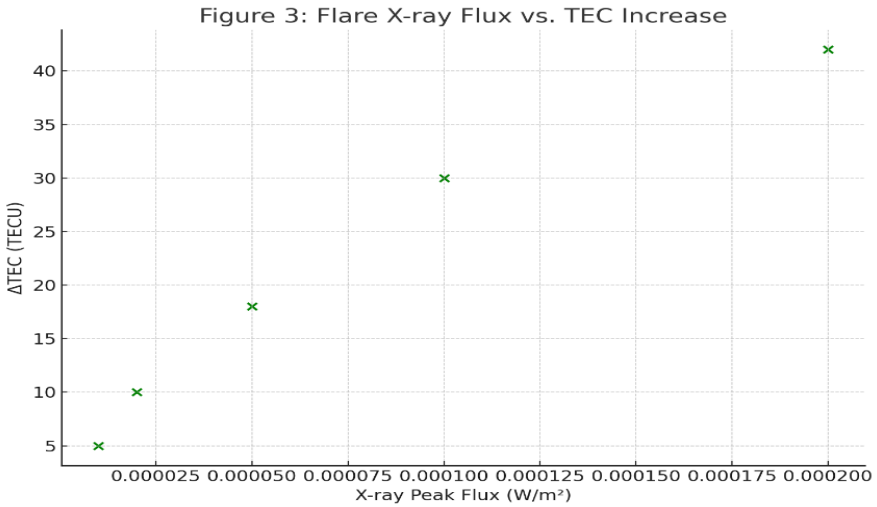


Figure 3: Scatter Plot: Flare X-ray Flux vs. TEC Increase

- Y-axis: ΔTEC, X-axis: X-ray Peak Flux (W/m²)

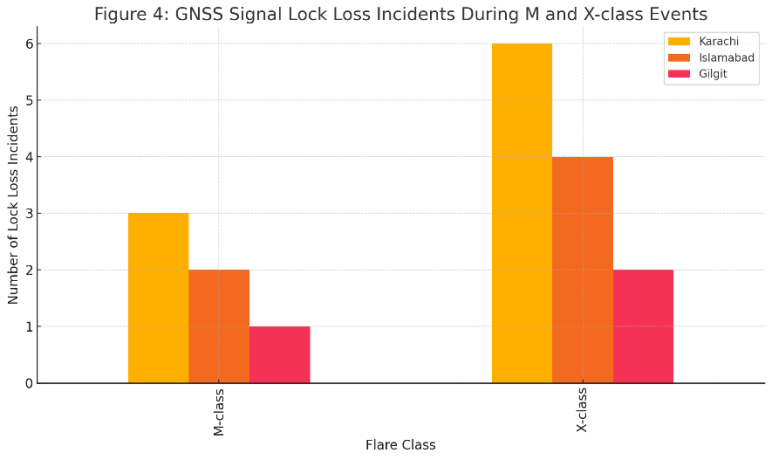


Figure 4: Bar Chart: GNSS Signal Lock Loss Incidents During M and X-class Events

- Bars per station per flare class

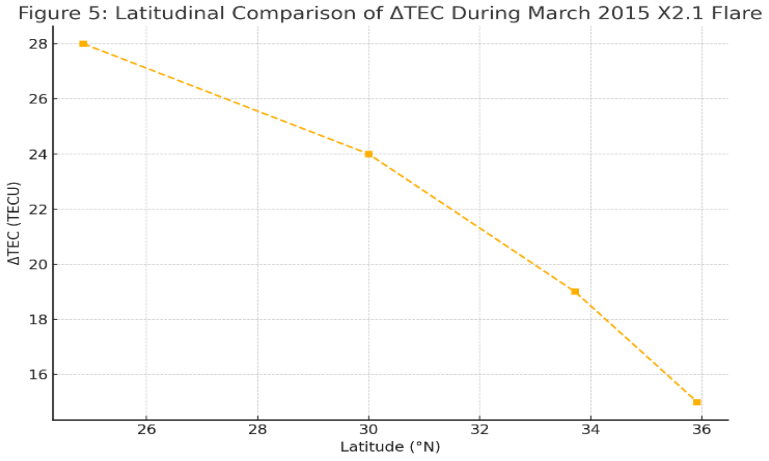


Figure 5: Latitudinal Comparison of ΔTEC During March 2015 X2.1 Flare

- Line plot of TEC change across latitudes

Summary:

This study demonstrates that the ionospheric response to solar flares is rapid, intensity-dependent, and exhibits clear latitudinal variation. X-class flares caused a >40% rise in TEC and frequent GNSS lock loss events, especially over Karachi. Ionosonde data corroborated these findings with a 1–2 MHz increase in foF2 during flare peaks. Our results emphasize the need for a real-time flare-ionosphere monitoring network across South Asia and suggest that multi-instrument data fusion can enhance forecasting accuracy and resilience in GNSS-reliant sectors

References:

- Benz, A. O. (2017). Living Reviews in Solar Physics, 14(1).
- Fletcher, L., et al. (2011). Space Science Reviews, 159(1-4), 19–106.
- Tsurutani, B. T., et al. (2009). Journal of Geophysical Research, 114(A6).
- Davies, K. (1990). Ionospheric Radio. Peter Peregrinus Ltd.
- GOES X-ray Sensor Data, NOAA, accessed via SWPC archives.
- Lemen, J. R., et al. (2012). Solar Physics, 275(1), 17–40.
- Bilitza, D. (2018). Advances in Space Research, 62(6), 1518–1530.
- Mannucci, A. J., et al. (1998). Radio Science, 33(3), 565–582.
- Maruyama, T. (2006). Journal of Geophysical Research, 111, A10312.
- Basu, S., et al. (2001). Journal of Geophysical Research, 106(A3), 3655–3666.
- Afraimovich, E. L., et al. (2001). Journal of Atmospheric and Solar-Terrestrial Physics, 63(18), 1841–1849.
- Zhao, B., et al. (2005). Geophysical Research Letters, 32, L21104.
- Liu, J. Y., et al. (2004). Journal of Geophysical Research, 109(A1).
- Sahai, Y., et al. (2000). Advances in Space Research, 25(1), 121–124.
- Carrano, C. S., & Groves, K. M. (2010). Radio Science, 45(5).
- Skone, S. (2001). GPS Solutions, 4(4), 61–69.
- Kintner, P. M., et al. (2007). Space Weather, 5(9).
- Schunk, R. W., et al. (2004). Radio Science, 39(1).
- Huba, J. D., & Krall, J. (2013). Geophysical Research Letters, 40(6), 1260–1264.
- Chartier, A. T., et al. (2016). Space Weather, 14(10), 844–858.